Alexandria Engineering Journal (2015) 54, 853–869

Alexandria University

Alexandria Engineering Journal

www.elsevier.com/locate/aej
www.sciencedirect.com

ORIGINAL ARTICLE

Modeling mixing convection analysis of discrete partially filled porous channel for optimum design

Mohamed G. Ghorab [1]

Ottawa, Canada

Received 24 May 2015; revised 27 June 2015; accepted 4 July 2015
Available online 14 August 2015

KEYWORDS

Mixing convection;
Heat transfer;
Prandtl number;
Nusselt number;
Darcy number;
Richardson number

Abstract Mixing convection flow inside a convergent horizontal channel partially filled with porous material and a clear channel are investigated numerically in the present study. Four discrete heat sources with uniform heat flux have been applied on the bottom surface of the channel. Three different channel exit heights are studied (H_e = 1, 0.5 and 0.25). The thermal and flow-field analysis inside the channel is investigated for different wide range of Reynolds number ($50 \leqslant Re \leqslant 300$), Darcy number ($10^{-2} \leqslant Da \leqslant 10^{-6}$), Richardson number ($0 \leqslant Ri \leqslant 100$) and Prandtl number ($0.7 \leqslant Pr \leqslant 10$). The present study carried out the effect of the channel exit height, Richardson number, Reynolds number, Darcy number and Prandtl number on the flow-field, the Nusselt number and the overall heat transfer performance. The Brinkman–Forchheimer–extended Darcy model is used to solve the governing equations of the fluid in the porous medium. The results reveal that the boundary layer thickness and flow velocity increase at high Richardson number for both porous and clear channels. The overall Nusselt number increases significantly for further increase in Darcy number, particularly for $Ri > 10$. The smallest channel exit height (H_e = 0.25) provides a high Nusselt number and low overall heat transfer performances. Furthermore, Richardson number has a small significant effect on overall Nusselt number and heat transfer performance at low Prandtl number.

1. Introduction

Enhancement heat transfer is vital in many thermal industrial applications such as; electrical machines cooling, macro and microelectronic equipments, refrigeration and air-conditioning, and gas flow heating in manufacturing and waste-heat recovery. In addition, it is required to increase the heat transfer rate in air and liquid cooling of engine and turbomachinery systems, sensible heating and cooling of viscous medium in thermal processing of chemical, pharmaceutical, and agricultural products. Therefore, improving the heat exchange performance increases significantly the thermal efficiency as well as the economics of the design and operation process. In order to enhance the heat transfer techniques, the thermal resistance in a conventional heat exchanger is reduced by promoting high convective heat transfer coefficient with or without increasing surface area. As a result, the heat exchanger size and the pumping power can be reduced. In addition, the

[1] On leave Department of Mechanical Engineering, Alexandria University, Alexandria, Egypt.
E-mail address: ghorabmg@gmail.com

Peer review under responsibility of Faculty of Engineering, Alexandria University.

http://dx.doi.org/10.1016/j.aej.2015.07.006

Nomenclature

C	inertial coefficient
C_p	specific heat at constant pressure (J/kg K)
Da	Darcy number
F	factor
Gr	Grashof number
H	inlet channel height (m)
h	heat transfer coefficient (W/m^2 K)
h_e	exit channel height (m)
H_e	dimensionless exit channel height (h_e/H)
H_p	dimensionless porous height (h_p/H)
h_p	porous height (m)
H_x	dimensionless local channel height (h_x/H)
h_x	local channel height (m)
K	permeability of the porous medium (m^2)
k_{eff}	effective thermal conductivity of the fluid-saturated porous medium (W/m K)
k_f	thermal conductivity of the fluid (W/m K)
Kr	thermal conductivity ratio (k_{eff}/k_f)
l	channel length (m)
L_I	dimensionless upstream unheated distance (l_i/H)
L_s	dimensionless distance between porous blocks (l_s/H)
l_s	distance between heat source (m)
N	total number of heat sources
Nu	Nusselt number
p	pressure (Pa)
P^*	pressure dimensionless
P_i	inlet pressure (Pa)
Pr	Prandtl number
q	uniform heat flux (W/m^2)
Ra	Rayleigh number
Re	Reynolds number
Ri	Richardson number
T	temperature (K)
u	main stream velocity (m/s)
U^*	dimensionless main stream velocity (u/u_i)
v	transverse velocity (m/s)
V^*	dimensionless transverse velocity (v/u_i)
w_p	porous block width (m)
W_p	dimensionless porous blocks width (w_p/H)
x, y	coordinates
X, Y	dimensionless coordinates (x/H, y/H)
X_{sn}	dimensionless heat sources centerlines (x_{sn}/H)

Greek symbols

Δ	difference between inlet and exit
α	thermal diffusivity of the fluid (m^2/s)
β	thermal expansion coefficient (K^{-1})
ε	porosity
θ	dimensionless temperature, $k_f(T - T_i)/qH$
θ_m	bulk temperature
θ_w	wall temperature, $k_f(T_w - T_i)/qH$
μ	dynamic viscosity (kg/m s)
μ_{eff}	effective dynamic viscosity (kg/m s)
μr	viscosity ratio
ν	kinematic viscosity (m^2/s)
ξ	overall heat transfer performance parameter
ρ	density (kg/m^3)

Subscripts

av	average
e	exit
eff	effective
f	fluid
i	inlet
m	bulk
p	porous
r	ratio
sn	heat source number (1, 2, 3 and 4)
w	wall
x	local

operating temperature of the heat exchanger can be decreased as well as increasing the heat duty of an existing exchanger.

The heat exchanger enhancement can be classified into passive and active techniques. The active technique required direct external power such as; surface and fluid vibrations, mechanical aids, injection, suction, jet impingement and electrostatic fields, while the passive technique required geometry modifications such as; rough, extended and treated the surfaces, swirl flow, surface tension devices, coiled tubes, and additives for liquid and gases.

Porous medium and transport are becoming vital in heat exchanger design in order to minimize the heat exchanger size with lower Reynolds number for small-scale applications such as electronic devices cooling. Huang and Vafai [1] studied the effect of porous block array on flow field and thermal characteristics of external laminar forced convection flow. They concluded that the presence of a porous block array near the boundary had significantly affected the convection characteristics. Hadim [2] studied numerically the effect of partially and fully filled porous channels using discrete heat source on the bottom wall. He reported that the enhancement in heat transfer is the same for the two cases when the width of the heat source is equal to the spacing between the porous layers for partially filled porous channel, whereas the partially filled porous channel provided low pressure drop (Δp) compared to fully filled channel. Sung et al. [3] studied numerically flow and heat transfer characteristics of forced convection in a channel which was partially filled with porous medium using Brinkman–Forchheimer–extended Darcy model. They reported that for fixed Darcy number (Da), the heat transfer enhanced as the thermal conductivity ratio (kr) increased. Also, the flow rate increased as porous block height (H_p) and Darcy number decreased. Moreover, the pressure drop increased as the porous block height increased and Darcy number decreased. In addition, Akam et al. [4] used Darcy–Brinkman–Forchheimer model to investigate transient forced convection in the developing region of parallel plate for a high thermal conductivity porous substrate. Their results showed that the highest Nusselt number (Nu) was achieved for fully porous duct. Furthermore, they observed that decreasing

Darcy number and increasing microscopic inertial coefficient (C) for high thermal conductivity had a significant effect on enhancement heat transfer rate. In addition, the microscopic inertial coefficient and the Darcy number had a higher effect on the thermal and hydrodynamic behavior of the flow compared to fully developed region. Fu et al. [5] investigated numerically laminar forced convection through a porous block mounted on a heated wall for different porous heights, porosity (ε), particle diameter and Reynolds number (Re). They concluded that the thermal performance enhanced for porous height of 0.5 with higher porosity value and particle diameter.

Jiang et al. [6] studied experimentally the effect of porous medium on heat transfer performance in micro heat exchanger. They reported that the porous medium enhanced the heat transfer rate and increased the pressure drop compared to micro-channel case. Bogdan and Abdulmajeed [7] reported based on their experimental and numerical studies that a high heat transfer rate could be achieved by inserting metallic porous materials inside the heat exchanger pipe with constant and uniform heat flux (q) at expense of reasonable pressure drop compared to the nonporous channel. Hetsroni et al. [8] investigated experimentally the heat transfer and the pressure drop performances for a rectangular channel by inserting sintered porous from stainless steel of different porosity. They reported that the sintered porous provided a high heat transfer efficiency with high pumping power compared to clear channel and the case with inserting compressed aluminum foams inside the channel. The convective heat transfer (h) and pressure drop (Δp) analysis in a channel with 90° turned flow using aluminum porous medium were investigated experimentally by Tzeng and Jeng [9]. The parameters studied were Reynolds number (Re) and the entry width to porous height ratio. They concluded that the average Nusselt number for 90° turned flow exceeded that for the straight channel at $Re < 1000$ but the straight channel ($H_e = 1$) provided higher average Nusselt number at $Re > 1000$ compared to 90° turned flow configuration. Moreover, the straight channel provided lower friction factor than that 90° turned flow channel.

Shokouhmand et al. [10] investigated the effect of porous thickness, Darcy number and the ratio of porous thermal to fluid conductivity on laminar flow and heat transfer characteristics between two parallel plates partially filled with a porous medium using Lattice Boltzmann Method (LBM). They reported that the Nusselt number increased by decreasing Darcy number at high conductivity ratio. Moreover, the optimum porous thickness increased with Darcy number and this conclusion was unaffected for fully filled porous channel case. Additionally, Javaran et al. [11] used the same method (LBM) to simulate the flow inside porous medium in order to analyze thermal characteristics of 2-D heat recovery system. They concluded that porous layers with high optical thickness and low scattering able to increase the recovering heat system coefficient for high temperature gases.

Li et al. [12] studied computationally fluid flow and heat transfer analysis in a channel with staggered porous blocks. They reported that the heat transfer enhanced at low Reynolds number (Re) with decreased Darcy number (Da) as the vortices were formed in the rear of each porous block, whereas, at high Reynolds number, the vortices between the porous blocks gradually diminished and the pressure drop increased. Moreover, there was a significant enhancement of the heat transfer at location of the porous blocks for further increase in the thermal conductivity ratio (Kr) between the porous blocks and the fluid. Wu and Wang [13] analyzed numerically unsteady convective heat transfer and flow characteristics for a heated square porous cylinder in a channel at different parameters studied including Darcy and Reynolds numbers. Their results showed that the local and total average Nusselt number increased as Reynolds and Darcy numbers increased but the porosity had a small influence on the heat transfer rate.

Venugopal et al. [14] investigated experimentally mixed convection heat transfer analysis in a vertical duct filled with metallic porous medium. They reported that for fixed Reynolds number, Nusselt number increased with decreasing the porosity (ε). Furthermore, Nusselt number achieved maximum value of 4.52 times that for a clear channel via using a porosity value of 0.85. Natural convection in a porous trapezoidal enclosure for uniform and non-uniform heated bottom wall was investigated numerically by Basak et al. [15] for different wide range of Darcy, Rayleigh, and Prandtl numbers (Da, Ra and Pr) as well as the inclination angle. They observed that the critical Ra numbers to the onset of convection were obtained at $Da = 10^{-3}$ for $Pr = 0.015$–1000. Moreover, the average Nusselt number increased exponentially for $Ra >$ critical Ra at $Da = 10^{-3}$. Inclination angle of 90° provided a high Nusselt number compared to other inclination angles.

Guerroudj and Kahalerras [16] simulated 2-D parallel plate channel with various porous block shapes to investigate the fluid flow and heat transfer characteristics of laminar mixed convective flow inside the channel using Brinkman–Forchheimer Darcy Model. The porous block configurations were rectangle, trapezoidal and triangular. They tested different parameter studies such as thermal conductivity (k), Reynolds number and porous medium permeability. They reported that the heat transfer rate was affected by vortices development which depended on Reynolds number, porous shape, thermal conductivity and permeability of the porous and the buoyancy force. The overall Nusselt number increased with the mixed convection parameter Gr/Re^2 for triangular shape at low permeability and Reynolds number, whereas, the rectangular shape provided a high heat transfer rate with a moderate increase of pressure drop at high thermal conductivity ratio and Reynolds and Darcy numbers.

1.1. Objective and parameter studies

Ghorab [17] studied the heat transfer of laminar forced convocation of convergent channel with different porous and exit channel heights. The present study is extended of Ghorab's [17] work to investigate flow-field and heat transfer analyses of laminar mixing convection for convergent partially filled porous channel and nonporous channel at different exit heights (H_e) and Prandtl numbers. The laminar mixing analysis of convergent porous channel at different Prandtl numbers did not exist in the literature. A wide range of different parameters are studied such as; the channel outlet height ($H_e = 0.25$, 0.5 and 1), Reynolds number ($50 \leqslant Re \leqslant 300$), Darcy number ($10^{-2} \leqslant Da \leqslant 10^{-6}$), Richardson number ($0 \leqslant Ri \leqslant 100$) and

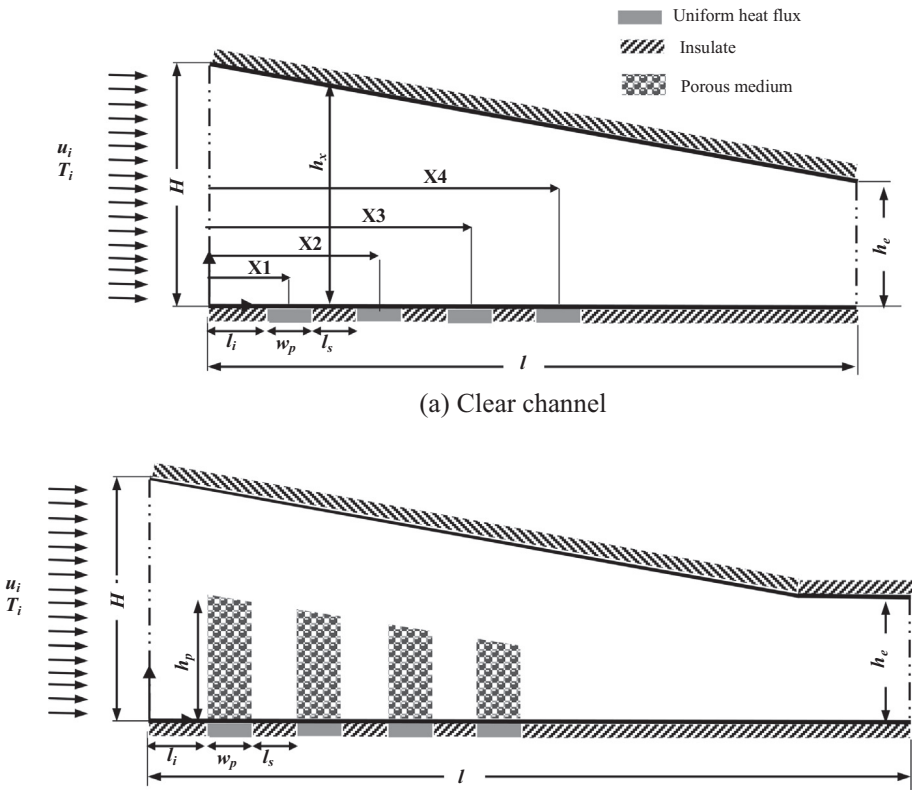

Figure 1 Schematic of the present nonporous and porous channels.

Prandtl number ($0.7 \leqslant Pr \leqslant 10$). The porous block height (H_p) is equal to 0.5 of the local channel height (H_x) and it has trapezoidal and rectangle shapes for convergent and straight channels, respectively. The porosity, thermal conductivity, viscosity ratio (μ_r) and inertial coefficient (C) have constant values of; $\varepsilon = 0.97$, $k = 1$, $\mu_r = 1$ and $C = 0.1$, respectively.

2. Mathematical methodology

Fig. 1 presents the computational domain of clear and porous channels with inlet height and length of H and L, respectively. The upper surface of the channel is thermally insulated and it has different inclination angles for varying the outlet height. Four discrete heat sources are applied on the bottom surface with uniform heat flux (q). The first heat source is located at distance of $l_i = 2H$. The heat source has a width of $w_p = H$ and it is equal to the space between two adjusted heat sources (l_s). The lower surface elsewhere (where there are no heat sources) is thermally insulated. A uniform velocity flow of u_i with constant temperature of T_i enters the channel. The straight and convergent channels have length of $20H$. An extra straight channel with length and height of $10H$ and H_e respectively is included downstream the convergent channel to confirm the fully developed conditions at the exit.

Different assumptions are considered through the present study in order to simplify the problem as follows: steady state, two-dimensional, incompressible flow, laminar flow, no external heat generation or sources and neglecting viscous dissipation.

Therefore governing equations can be presented as follows:

- ***Continuity equation:***

$$\frac{\partial u}{\partial x} + \frac{\partial v}{\partial y} = 0 \tag{1}$$

u and v are flow velocity in x and y directions, respectively and x and y are coordinates.

- ***Momentum equations:*** in X direction:

$$\frac{\rho}{\varepsilon^2}\left(u\frac{\partial u}{\partial x} + v\frac{\partial u}{\partial y}\right) = -\frac{\partial p}{\partial x} + \mu\left(\frac{\partial^2 u}{\partial x^2} + \frac{\partial^2 u}{\partial y^2}\right) - \frac{F\mu_f}{K}u - \frac{FC\rho}{\sqrt{K}}|\vec{V}|u \tag{2}$$

where ρ, μ and P are density, dynamic viscosity and pressure of the flow, respectively. F is a coefficient and has value of 0 and 1 for the fluid and the porous media, respectively. In addition, $\varepsilon = 1$ for the fluid medium and it has range of $0 < \varepsilon < 1$ for the porous medium.

$$|\vec{V}| = \sqrt{u^2 + v^2}$$

in Y direction:

$$\frac{\rho}{\varepsilon^2}\left(u\frac{\partial v}{\partial x} + v\frac{\partial v}{\partial y}\right) = -\frac{\partial p}{\partial y} + \mu\left(\frac{\partial^2 v}{\partial x^2} + \frac{\partial^2 v}{\partial y^2}\right) - \frac{F\mu_f}{K}v - \frac{FC\rho}{\sqrt{K}}|\vec{V}|v + \rho g\beta\Delta T \tag{3}$$

where g, β and ΔT are gravitational acceleration, thermal expansion coefficient and temperature difference, respectively.

– ***Energy equation***

$$\text{for fluid } (f)\quad \rho C_p\left(u\frac{\partial T}{\partial x}+v\frac{\partial T}{\partial y}\right) = \frac{\partial}{\partial x}\left(k_f\frac{\partial T}{\partial x}\right)+\frac{\partial}{\partial y}\left(k_f\frac{\partial T}{\partial y}\right)+h(T_f-T_p) \tag{4a}$$

$$\text{for porous } (p)\quad \rho C_p\left(u\frac{\partial T}{\partial x}+v\frac{\partial T}{\partial y}\right) = \frac{\partial}{\partial x}\left(k_{eff}\frac{\partial T}{\partial x}\right)+\frac{\partial}{\partial y}\left(k_{eff}\frac{\partial T}{\partial y}\right) \tag{4b}$$

Boundary condition:

• ***At channel inlet:***

$$\text{At } x=0\ \&\ 0<y<H:\quad u=u_i, v=0 \text{ and } T=T_i \tag{5}$$

• ***At channel exit:***

The velocity and temperature gradients are tested at different locations of $x > 13H$ for straight channel and $x > 24H$ for convergent channels. From the results, there is no change in temperature and velocity gradient along the downstream direction. Therefore, fully developed conditions are assumed at the channel exit in the present study.

$$\text{At } x=l\ \&\ 0<y<h_e: \frac{\partial u}{\partial x}=\frac{\partial T}{\partial x}=0 \text{ and } v=0. \tag{6}$$

• ***At upper surface:***

$$\text{At } y=h_x\ \&\ 0<x<l: u=v=0, \text{ and } \frac{\partial T}{\partial y}=0. \tag{7}$$

• ***At lower surface:***

$$y=0\ \&\ 0<x<l: u=v=0,$$
$$q=-k_{eff}\frac{\partial T}{\partial y} \text{ (at the heat source location) and}$$
$$\frac{\partial T}{\partial y}=0 \text{ (elsewhere).} \tag{8}$$

Non-dimensional terms:

The following dimensionless terms are used in order to present the governing equations in dimensionless form:

$$\left.\begin{array}{l} X=\frac{x}{H},\quad Y=\frac{y}{H},\quad H_e=\frac{h_e}{H},\quad H_x=\frac{h_x}{H},\quad L_l=\frac{l_l}{H},\\ L_S=\frac{l_s}{H},\quad W_p=\frac{w_p}{H},\quad H_p=\frac{h_p}{H},\quad V^*=\frac{v}{u_i},\quad U^*=\frac{u}{u_i},\\ Kr=\frac{k_{eff}}{k_f},\quad P^*=\frac{(P-P_i)}{\rho u_i^2},\quad Pr=\frac{\nu}{\alpha},\quad \theta=\frac{T-T_i}{qH/k_f},\\ \theta_m=\frac{T_m-T_i}{qH/k_f},\quad \theta_w=\frac{T_w-T_i}{qH/k_f},\quad \mu_r=\frac{\mu_{eff}}{\mu_f},\quad Da=\frac{K}{H^2},\end{array}\right\}$$

$$Re=\frac{\rho u_i H}{\mu_f},\quad Gr=\frac{g\beta\frac{qH}{k_f}H^3}{\nu^2},\quad Ri=\frac{Gr}{Re^2}. \tag{9}$$

where k_{eff} and μ_{eff} are effective (fluid-saturated porous medium) of thermal conductivity and dynamic viscosity, respectively. "θ" is non-dimensional temperature.

The governing equations in dimensionless form are presented as follows:

– ***Continuity equation:***

$$\frac{\partial U^*}{\partial X}+\frac{\partial V^*}{\partial Y}=0 \tag{10}$$

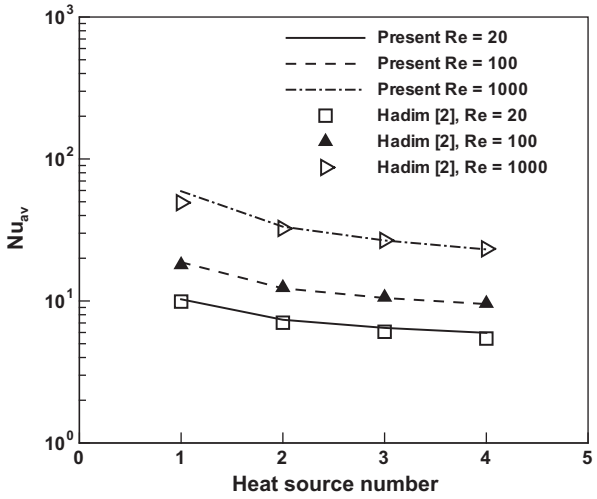

(a) Clear channel

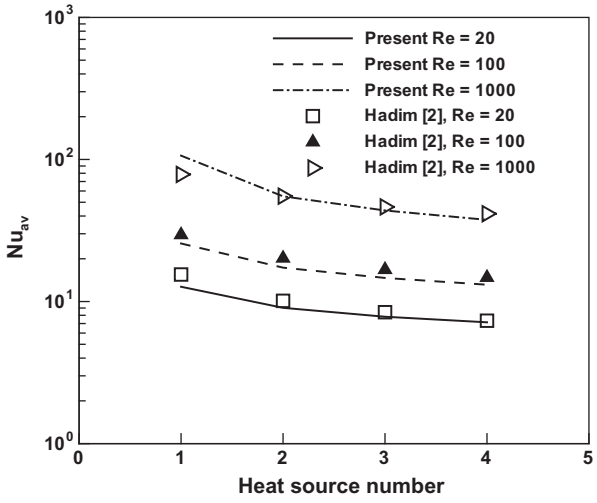

(b) Partially porous channel (Da = 10^{-3})

Figure 2 Nusselt number variation in porous and clear channels for validation study.

– ***Momentum equation:***

$$\frac{1}{\varepsilon^2}\left(U^*\frac{\partial U^*}{\partial X}+V^*\frac{\partial U^*}{\partial Y}\right)=-\frac{\partial P^*}{\partial X}+\frac{\mu_r}{Re}\left(\frac{\partial^2 U^*}{\partial X^2}+\frac{\partial^2 U^*}{\partial Y^2}\right)-\frac{F}{ReDa}U^*-\frac{F*C}{\sqrt{Da}}|\vec{V}^*|U^* \tag{11}$$

$$\frac{1}{\varepsilon^2}\left(U^*\frac{\partial V^*}{\partial X}+V^*\frac{\partial V^*}{\partial Y}\right)=-\frac{\partial P^*}{\partial Y}+\frac{\mu_r}{Re}\left(\frac{\partial^2 V^*}{\partial X^2}+\frac{\partial^2 V^*}{\partial Y^2}\right)-\frac{F}{ReDa}V^*-\frac{F*C}{\sqrt{Da}}|\vec{V}^*|V^*+Ri\theta \tag{12}$$

– ***Energy equation:***

$$\left(U^*\frac{\partial\theta}{\partial X}+V^*\frac{\partial\theta}{\partial Y}\right)=\frac{kr}{Pr\ Re}\left(\frac{\partial^2\theta}{\partial X^2}+\frac{\partial^2\theta}{\partial Y^2}\right)+\frac{(1-F)}{Pr\ Re} \tag{13}$$

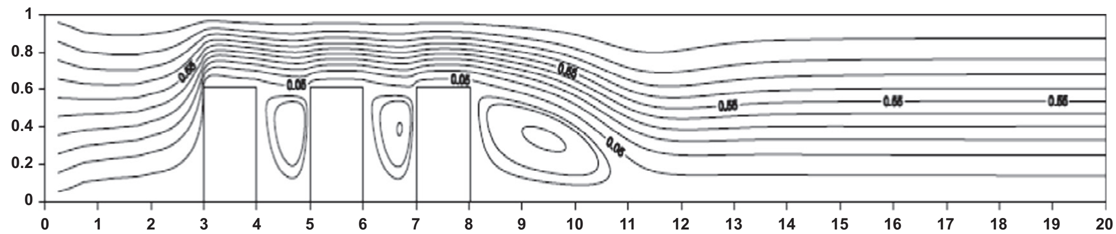

(a) Guerroudj and Kahalerras [16]

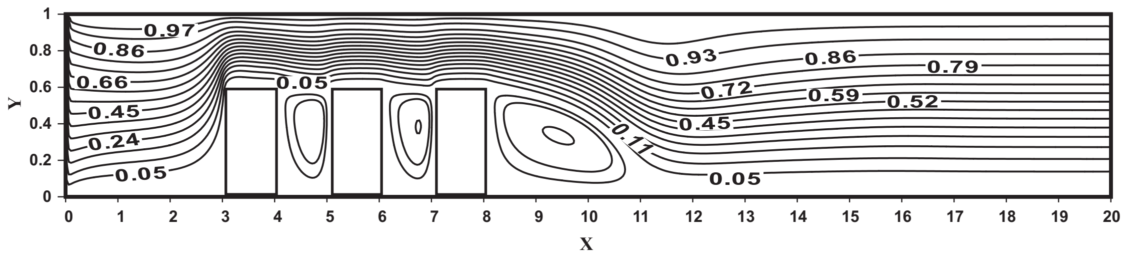

(b) Present study

Figure 3 Streamline similarity comparison between the present result and Guerroudj and Kahalerras [16] for rectangular porous blocks at $Re = 100$, $Da = 10^{-6}$, $Hp = 0.6$ and $kr = 1$.

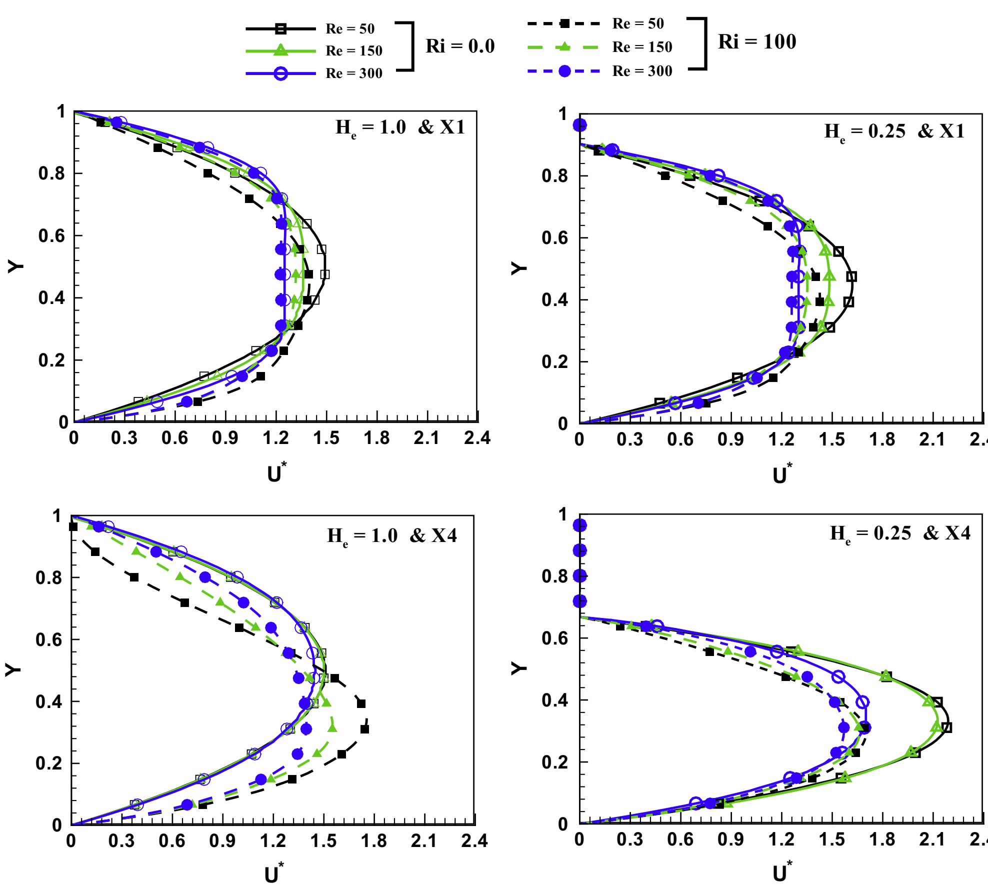

Figure 4 Streamwise velocity profiles at X1 and X4 for different Reynolds and Richardson numbers and exit height for clear channel.

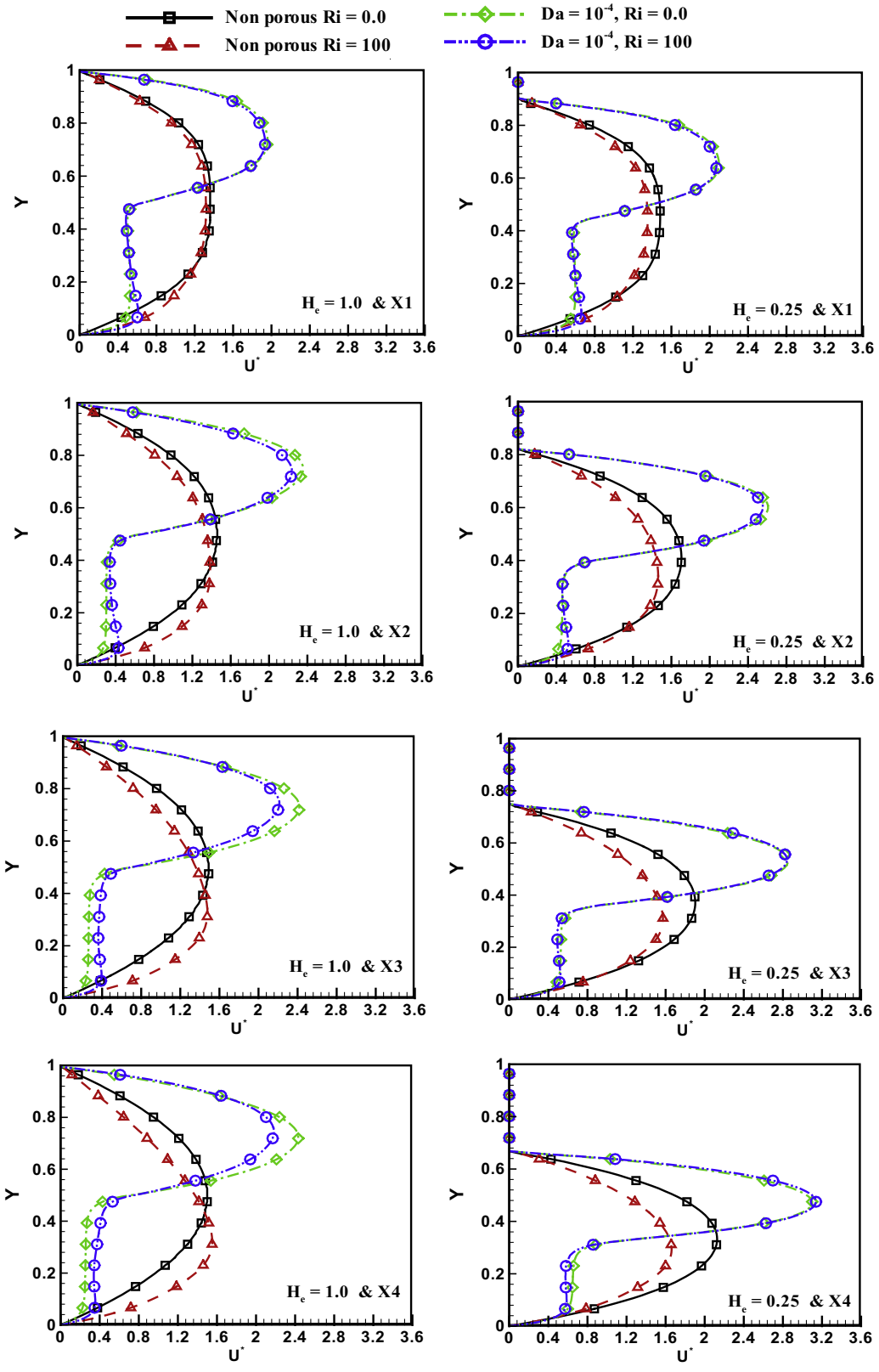

Figure 5 Streamwise velocity profiles at heat source centers for clear and porous channels at different *He* and *Ri* (*Re* = 150).

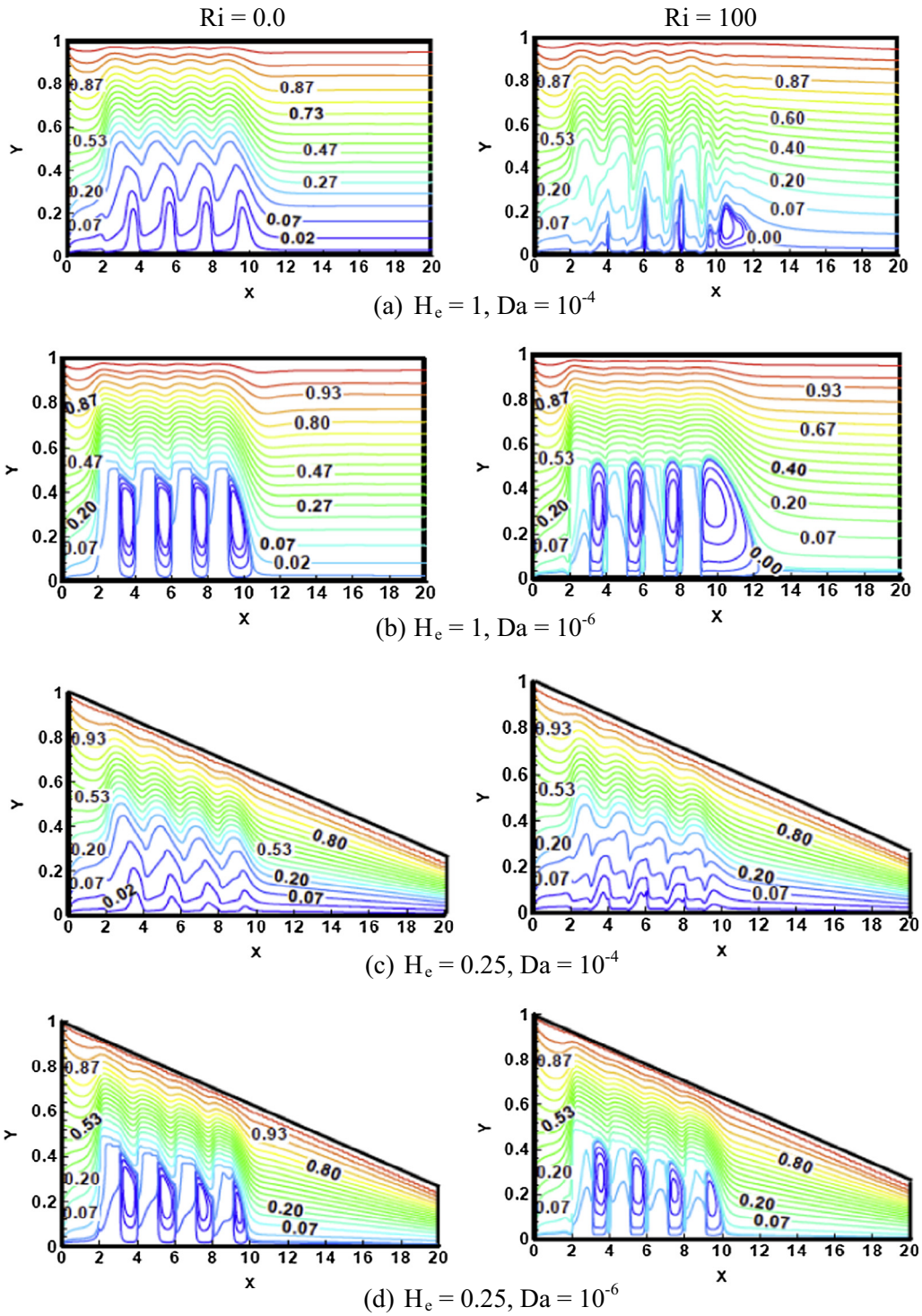

Figure 6 Effect of Richardson number on flow pattern for porous channel with different outlet heights and Darcy numbers ($Re = 50$).

For fluid region, $\mu_r = Kr = 1$ and $F = 0$ and for porous region; $F = 1$, $0 < \mu_r < 1$ and $0 < kr < 1$.

Boundary condition in dimensionless form:

- ***At channel inlet:***

$$\text{At } X = 0 \text{ and } 0 < Y < 1 : U^* = 1 \text{ and } V^* = \theta = 0 \tag{14}$$

- ***At channel exit:***

$$\text{At } X = L \text{ and } 0 < Y < H_e : V^* = 0 \text{ and } \frac{\partial U^*}{\partial X} = \frac{\partial \theta}{\partial X} = 0 \tag{15}$$

- ***At upper surface:***

$$\text{At } Y = H_x \text{ and } 0 < X < L : U^* = V^* = 0 \text{ and } \frac{\partial \theta}{\partial Y} = 0 \tag{16}$$

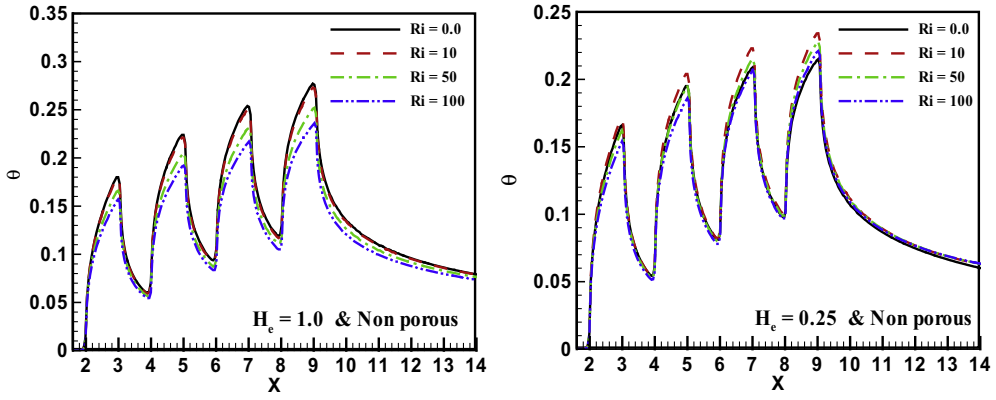

(a) Non porous channel

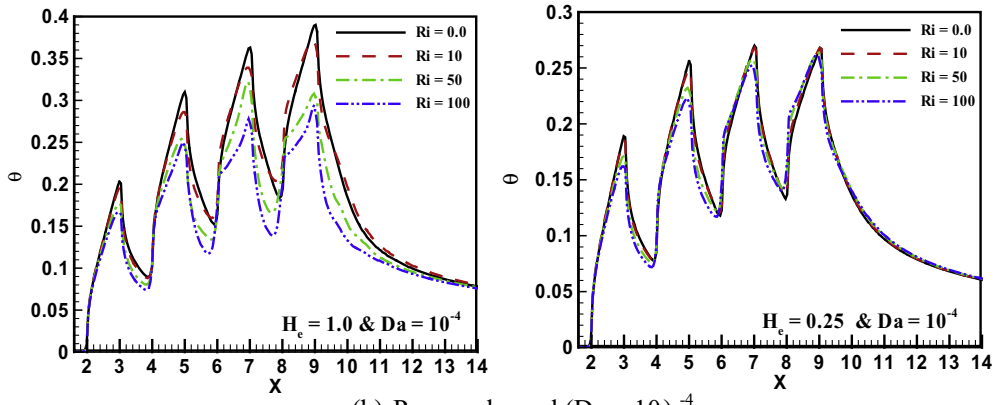

(b) Porous channel (Da = 10) $^{-4}$

Figure 7 Surface temperature variation along downstream for different *Ri* and *He* at *Re* = 150; (a) non porous channel (b) porous channel.

• ***At lower surface:***

$$\text{At } Y = 0 \text{ and } 0 < X < L : U^* = V^* = 0 \text{ and,}$$
$$\left.\begin{array}{ll} \frac{\partial\theta}{\partial Y} = 0 & \text{(for adiabatic surfaces),} \\ \frac{\partial\theta}{\partial Y} = \frac{-1}{K_k} & \text{(at heat sources).} \end{array}\right\} \quad (17)$$

Calculated parameters:

Different local and average dimensionless physical parameters are calculated in Eqs. (18)–(22) and used in the present results.

– The local bulk temperature:

$$\theta_m = \frac{\int_0^{H_x} |U^*|\theta dY}{\int_0^{H_x} |U^*| dY} \quad (18)$$

– The local Nusselt number:

$$Nu = \frac{qH}{k_f(T_w - T_m)} = \frac{1}{\theta_w - \theta_m} \quad (19)$$

T_w and T_m are wall and main temperatures, respectively.

– The average Nusselt number over the heat source:

$$\overline{Nu}_{sn} = \frac{1}{W_p} \int_{X_{sn}-\frac{W_p}{2}}^{X_{sn}+\frac{W_p}{2}} Nu\, dX \quad (20)$$

where *sn* is heat source number (*sn* = 1, 2, 3 and 4) and W_p is heat source width.

– The overall Nusselt number:

$$\overline{\overline{Nu}} = \frac{\sum_{sn=1}^{sn=N} \overline{Nu}_{sn}}{N} \quad (21)$$

N is the total number of heat sources (*N* = 4).

The overall heat transfer performance (ξ) is defined as ratio of heat dissipation to pumping power [18]:

$$\xi = \frac{\overline{\overline{Nu}}}{\Delta P^* Re^3} \quad (22)$$

3. Numerical procedure

The governing equations are solved numerically using finite volume method. The FORTRAN language is used in the present programming code. The solving technique is based on the discretization of the governing equations using the central difference in space. The power law scheme is used in the discretizing procedure with a linear profile between the velocity values in the center of the mesh, and those of the neighboring nodes. The velocity and the pressure fields are linked by the SIMPLE algorithm which was used by Patanker [19]. The inclined upper surface is simulated by a series of rectangular steps (blocking

off operation) which was proposed by Patanker [19]. Four different grids sizes are tested for grids independence investigation. The grids size of 420 × 100 is used in the present study as the difference in the results between used grids sizes and the finest grids is less than 0.5%. The grids are designed to be intensive near the bottom surface as well as near the porous blocks. The iteration method used in the program is a line-by-line procedure, which is a combination of the direct method and the resulting Tri Diagonal Matrix Algorithm (TDMA). The iteration number of 20,000 is used in the present study to provide a relative variation between two successive iterations less than 10^{-5} and 10^{-4} for the velocity and the temperature, respectively at different tested locations.

Fig. 2a and b demonstrates validation study for both clear and partially filled porous channels, respectively. The average Nusselt number over each heat source obtained by Hadim [2] is compared with the present results at $Da = 10^{-3}$, $H_p = 1$, $L_I = 3$, $W_p = L_s = 1$, $\varepsilon = 0.97$, $C = 0.1$ and $Re = 20$, 100 and 1000. From the results, there is a good agreement with accuracy more than 95% for both clear and partially porous channels. In addition, a channel with three heat sources and rectangular porous blocks studied by Guerroudj and Kahalerras [16] is simulated for validation study. Fig. 3 shows comparison between the present streamlines and that was obtained by Guerroudj and Kahalerras [16] at $Re = 100$, $Da = 10^{-6}$, $H_p = 0.6$ and $kr = 1$. The results show that there is an excellent agreement between the two streamline figures. As a result, the current code and methodology can be utilized for further heat transfer and fluid flow analyses for porous and clear channels with heated sources.

4. Results and discussion

4.1. Flow-field

Fig. 4 demonstrates the effect of Reynolds and Richardson numbers on the streamwise velocity profiles at X1 and X4 (center of the first and the last heat sources) for the clear channel with different outlet heights. The result shows that the velocity profile has parabolic shape along streamwise direction at low Reynolds number for $H_e = 1$ and 0.25. The velocity profile becomes a flat at the channel centerline for further increase in Reynolds number at location near the channel inlet (X1). Moreover, the velocity decreases by increasing Richardson number at low and high Reynolds numbers for $H_e = 1$ and 0.25 at X1 (in Fig. 4a and b) and at X4 for $H_e = 0.25$ (in Fig. 4c). Furthermore, a high Richardson number provides less boundary layer thickness near the bottom surface for straight channel ($H_e = 1.0$) at X1 and X4 (Fig. 4a and c). In addition, at X4 the peak velocity moves near the bottom surface for straight channel by increasing Richardson number at low Reynolds number, whereas, Richardson number has no

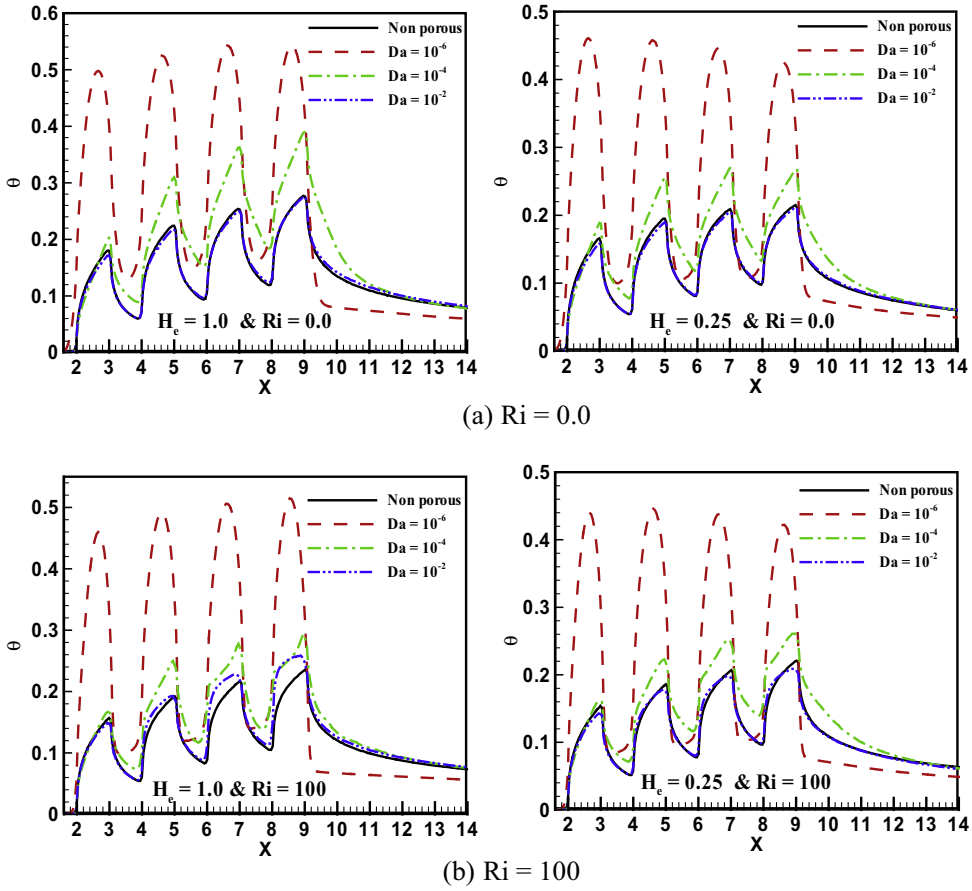

Figure 8 Surface temperature variation along downstream at different *Da* and *He* for porous and clear channels ($Re = 150$); (a) $Ri = 0$, and (b) $Ri = 100$.

significant effect on boundary layer at X4 for convergent channel (H_e = 0.25), as presented in Fig. 4d.

Fig. 5 shows the streamwise velocity profiles at the heat source centerlines (X1, X2, X3 and X4) for porous and nonporous channels at H_e = 1 and 0.25 for Re = 150. From the results, the Richardson number has significant effect on the boundary layer thickness for porous and clear channels along streamwise direction. For straight channel, at high Richardson number the boundary layer thickness decreases. Moreover, the boundary layer thickness is higher in the porous channel compared to clear channel at the same Richardson number. The velocity value above the porous blocks decreases at high Richardson number for straight channel with significant effect further downstream, whereas, the velocity across the porous blocks for $Y < 0.5$ increases for straight channel by increasing Richardson number along the downstream direction, as shown in Fig. 5 (on left). On the other hand, Richardson number has no significant effect on the velocity flow profile for porous convergent channel (H_e = 0.25) along the streamwise direction as presented in Fig. 5 (on right). However, the velocity decreases for clear convergent channel for further increase in Richardson number.

Effect of Richardson number on streamlines for different exit heights and Darcy numbers at Re = 50 is illustrated in Fig. 6. A circulation flow is observed downstream the porous blocks for further increase in Richardson number for straight channel at $Da = 10^{-4}$, as shown in Fig. 6a. Therefore, the convective heat transfer enhances and reduces the surface wall temperature. The flow circulation is created in the rear of the porous blocks at low Ri and $Da = 10^{-6}$, as illustrated in Fig. 6b. However, there is no significant effect of increasing Richardson number on flow pattern for convergent channel (H_e = 0.25) at $Da = 10^{-4}$, as presented in Fig. 6c. The reason for that is because the convergent channel accelerates the flow in the streamwise direction. The flow circulation can be observed at $Da = 10^{-6}$ for convergent porous channel for H_e = 0.25 with small significant enhancement effect at Ri = 100, as shown in Fig. 6d.

4.2. Temperature performance

Fig. 7 presents surface temperature variation for clear and porous channels at Re = 150 for different Richardson numbers. The results show that, there is no significant effect on the surface temperature at $Ri \leqslant 10$ for nonporous straight channel, as shown in Fig. 7a (on left), whereas, the surface temperature decreases significantly over the heat sources for clear and porous straight channels at $Ri \geqslant 50$ with more significant effect further downstream, as presented in Fig. 7a and b (on left). On the other hand, Richardson number has a small significant

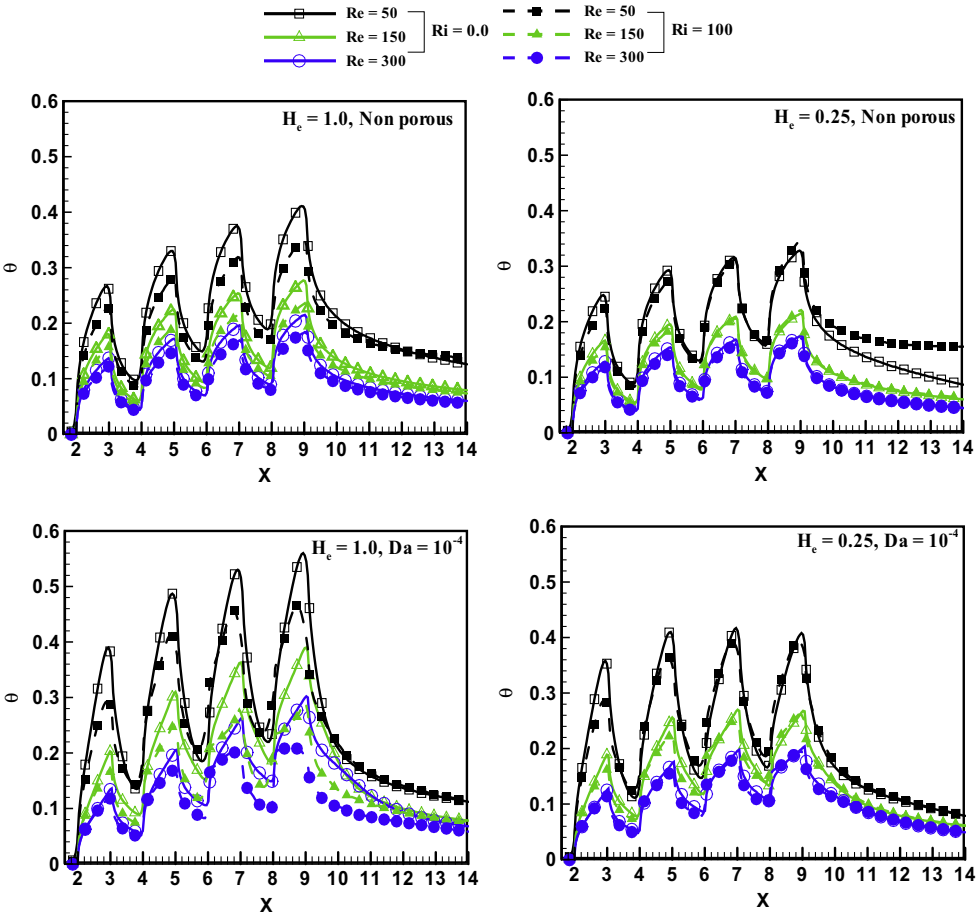

Figure 9 Effect of Reynolds number on surface temperature for clear and porous channels at He = 1.0 and 0.25 ($Da = 10^{-4}$).

effect on the surface temperature for clear and porous convergent channels. The temperature profile over the first heat source has the lowest values compared to the temperature profiles over other heat sources as the first heat source is exposed to the lowest temperature ($\theta = 0$). The temperature profile has the highest values over the fourth heat source for clear straight and convergent channels as well as porous straight channel, while, the temperature profiles over the last two heat sources (X3 and X4) have the same profile for porous convergent channel, as illustrated in Fig. 7b (on right). In general, the temperature distribution over the bottom surface has a sawtooth-shape. The peak temperature values over the heat sources decrease at high Richardson number. As a result, the temperature decreases for $H_e = 0.25$ due to increasing the forced convective heat transfer over the bottom surface compared to the straight channel. In addition, inserting porous medium inside the channel affects significantly on temperature distribution over the bottom surface especially for straight channel at $Ri > 10$, as shown in Fig. 7b (on left).

The effect of Darcy number on temperature distribution for straight and convergent channels ($H_e = 1$ and 0.25) at $Re = 150$ for different Richardson numbers ($Ri = 0$ and 100) is presented in Fig. 8. The results show that the temperature profile over the downstream surface decreases significantly for further increase in Darcy number at $Ri = 0$ and 100 for both straight and convergent channels. At $Ri = 0$, the porous channel with $Da = 10^{-2}$ provides the same temperature performance as the clear channel for both straight and convergent channels, as presented in Fig. 8a. Moreover, there is no significant effect by including porous blocks with $Da = 10^{-2}$ at $Ri = 100$ on temperature distribution, as shown in Fig. 8 (on right). Additionally, for $Da > 10^{-4}$, there is no significant effect on surface temperature distribution; over the first heat source at $Ri = 0$ and 100 for straight and convergent channels, as illustrated in Fig. 8. The porous channel with $Da = 10^{-6}$ provides the highest temperature values at $Ri = 0$ and 100.

Fig. 9 presents the effect of Reynolds number on the surface temperature distribution for clear and porous channels at $Ri = 0$ and 100, $H_e = 1$ and 0.25. The surface temperature significantly decreases for further increase in Reynolds number and decreases more at high Richardson number particularly for clear and porous straight channels, as shown in Fig. 9a and c (on left). Moreover at $Re > 50$, the temperature decreases significantly at high Richardson number over the heat sources of $sn = 2$, 3 and 4 for straight porous channel,

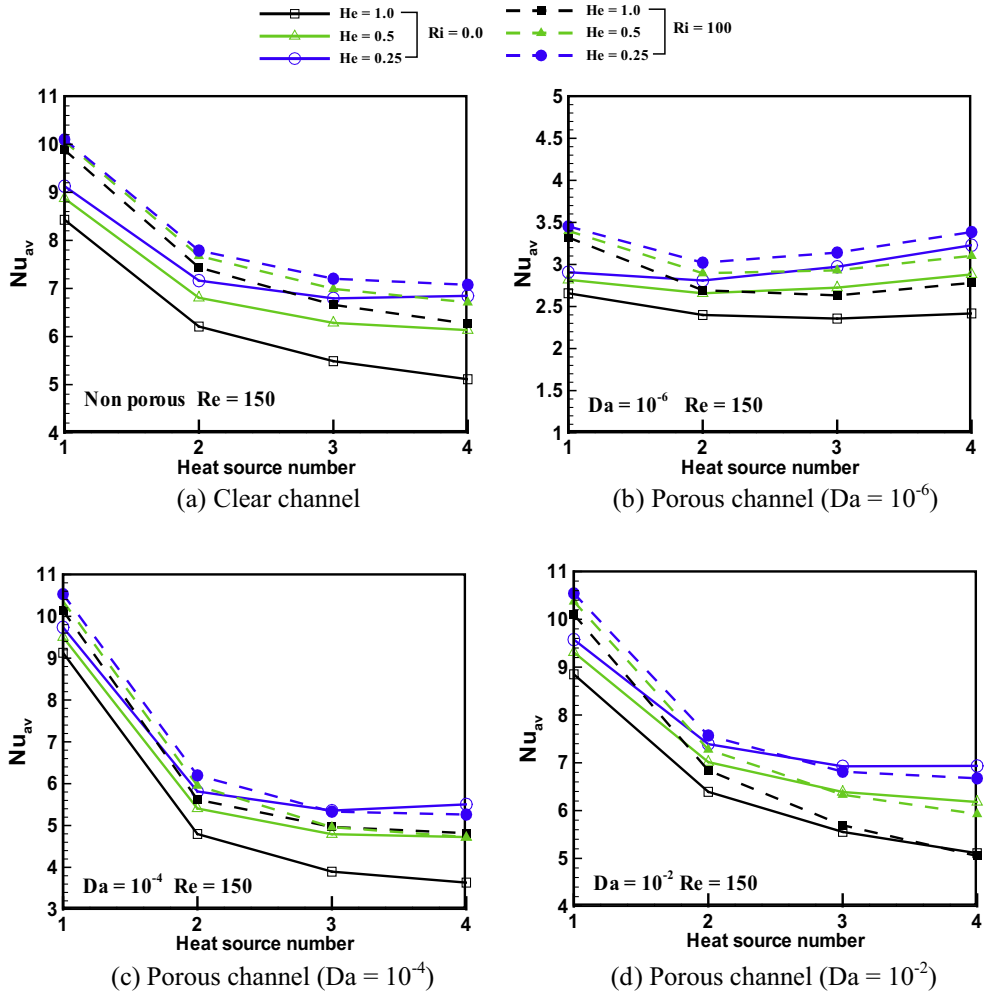

(a) Clear channel (b) Porous channel (Da = 10^{-6})

(c) Porous channel (Da = 10^{-4}) (d) Porous channel (Da = 10^{-2})

Figure 10 Average Nusselt number variation over the heat sources at different He and Ra for clear and porous channels ($Re = 150$).

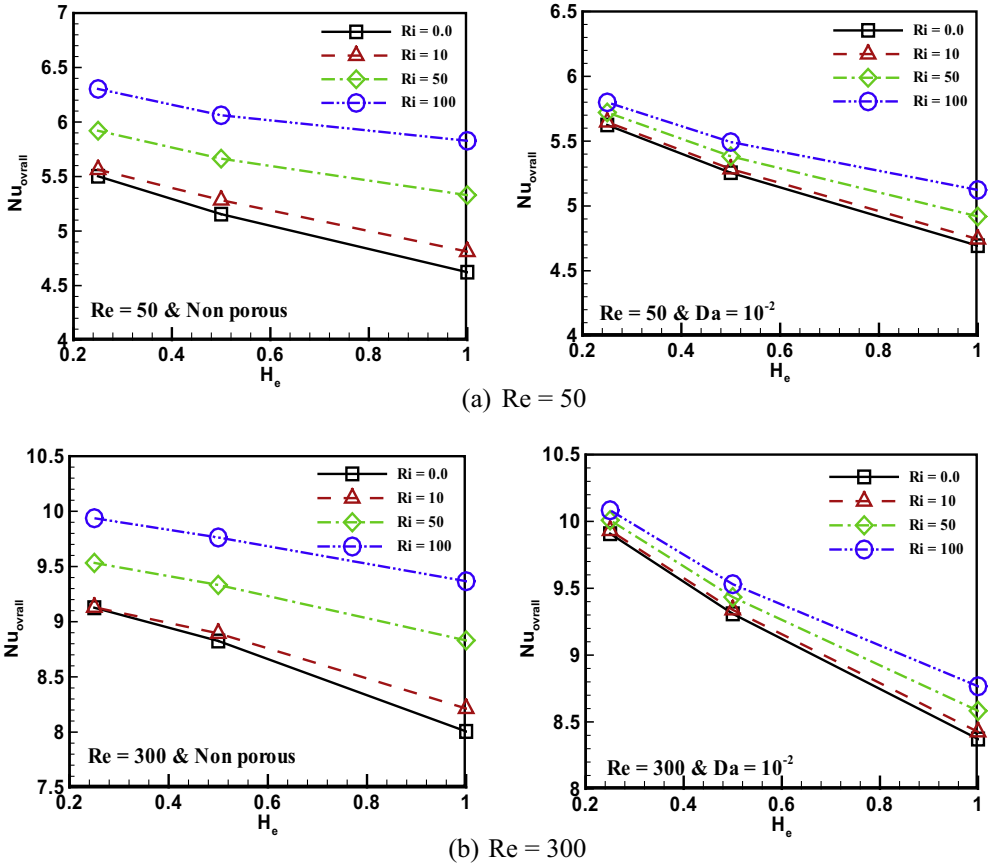

Figure 11 Variation of overall Nusselt number with exit height at different Richardson number for clear and porous channels, $Re = 50$ and 300, $Da = 10^{-2}$.

as shown in Fig. 9c. Moreover, the surface temperature decreases for further increase in Reynolds number for convergent clear and porous channels without significant effect of Richardson number, as presented in Fig. 9b and d. The peak temperatures over heat source ($sn = 2$, 3, and 4) are almost the same for porous convergent channel at different Reynolds numbers, as illustrated in Fig. 9d, whereas, the peak temperature has the highest value over the last heat source ($sn = 4$) at low Reynolds number for other case studies, as shown in Fig. 9a–c.

4.3. Nusselt number

Fig. 10 illustrates the average Nusselt number distribution over each heat source for clear and porous channels at different outlet heights and Richardson numbers for $Re = 150$. The results show that small exit channel height enhances the average Nusselt number over the heat sources compared to straight channel with more significant effect further in streamwise direction. Nusselt number has the highest value near the channel inlet and decreases gradually along the streamwise direction for $H_e = 0.25$ for clear channel and porous channels with $Da \geqslant 10^{-4}$, as shown in Fig. 10a, c and d, whereas, Nusselt number has the highest value over the last heat source ($sn = 4$) for porous channel at $Da = 10^{-6}$ (Fig. 10b). In addition, the average Nusselt number over the heat sources is almost the same for the channel with exit height of $H_e = 1$ and 0.5 at $Ri = 0$ and $Da = 10^{-6}$. The average Nusselt number enhances for further increase in the Richardson number with significant effect near the channel entrance for clear channel and porous channel with $Da \geqslant 10^{-4}$. The Richardson number has a small effect on the average Nusselt number further downstream the convergent channel.

Fig. 11 presents the overall Nusselt number variation with the channel outlet height over the four heat sources at different Richardson numbers ($0 \leqslant Ri \leqslant 100$) and Reynolds number ($Re = 50$ and 300) for porous channel ($Da = 10^{-2}$) and clear channel. The results show that the overall Nusselt number has a high value for small exit height and decreases gradually for further increase in the channel exit height at low and high Reynolds numbers. For $Ri > 10$, there is a significant increase in the overall Nusselt number for clear channel. The overall Nusselt number enhances for the clear channel at $Re = 50$ due to increase in Richardson number from $Ri = 0$–100 by ≈14% and ≈27% for $H_e = 0.25$ and 1 respectively, as shown in Fig. 11a (on left), while, the enhancement in overall Nusselt number at $Re = 300$ for clear channel is approximately 9% and 23% for $H_e = 0.25$ and 1, respectively due to increase in Richardson number, as presented in Fig. 11b (on left). Moreover, increasing Richardson number enhances the overall Nusselt number of the porous channel ($Da = 10^{-2}$) by 2% and 11% at $Re = 50$ in addition to 5% and 20% at $Re = 300$ for $H_e = 0.25$ and 1, respectively.

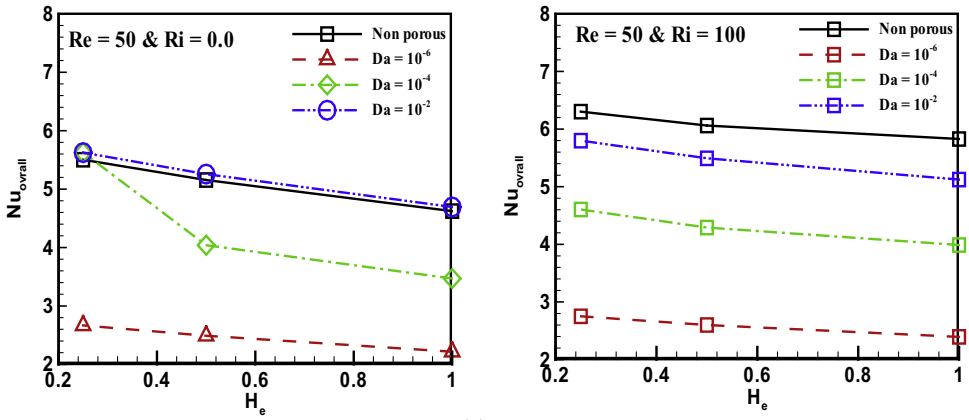

(a) Re = 50

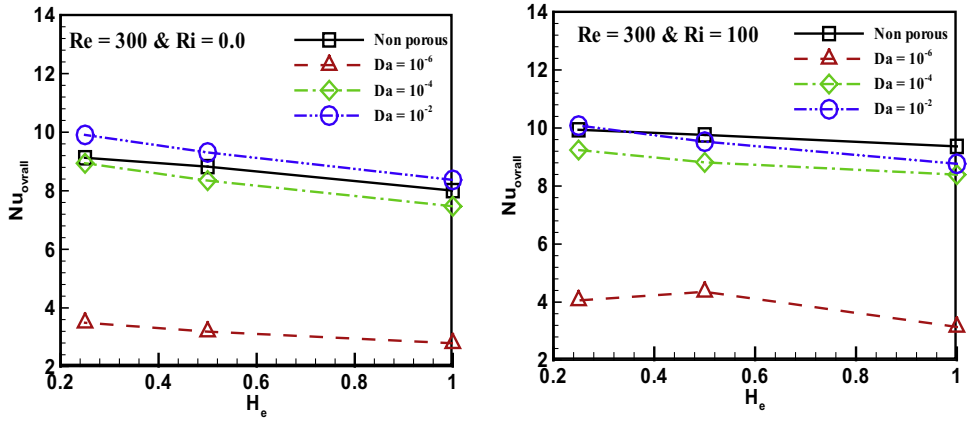

(b) Re = 300

Figure 12 Variation of overall Nusselt number with exit height for clear and porous channels at different Darcy number (Ri = 0 and 100); (a) Re = 50, and (b) Re = 300.

Furthermore, the overall Nusselt number at Re = 300 has value of ≈1.6 and 1.72 times that at Re = 50 for clear and porous channels, respectively.

The overall Nusselt number variation with channel exit height for different Darcy numbers ($10^{-6} \leqslant Da \geqslant 10^{-2}$) as well as clear channel is illustrated in Fig. 12 at Re = 50 and 300 and Ri = 0 and 100. The result shows that the porous medium with $Da = 10^{-6}$ provides the lowest overall Nusselt number among other cases studied at low and high Reynolds numbers. The overall Nusselt number enhances for further increase in Darcy and Reynolds numbers. Moreover, the convergent channel with exit height of 0.25 provides the maximum overall Nusselt number and the straight channel produces the lowest overall Nusselt number values under the same conditions. In addition, the results show that Richardson number enhances the overall Nusselt number more at low Reynolds number for clear and porous channels with respect to high Reynolds number, as shown in Fig. 12.

4.4. Overall heat transfer performance

The overall heat dissipation from the heat sources compared to pumping power consumption is evaluated in the present study using overall heat transfer performance parameter, as presented in Eq. (22). Fig. 13 shows the overall heat transfer variation with channel outlet height at different Richardson numbers for clear and porous channels. From the results, the straight channel provides the highest overall heat transfer performance (ξ) and it decreases by reducing the channel outlet height. In addition, Richardson number has significant effect on overall heat transfer performance for clear straight channel. The maximum overall heat transfer value is achieved at Ri = 100 and low Reynolds number (Re = 50). Moreover, there is no significant effect for $Ri \geqslant 10$ on overall heat transfer performance for porous and clear convergent channels (H_e = 0.5 and 0.25). The overall heat transfer performance decreases at high Reynolds number due to increase in the pressure drop across the channel which increases the pumping power.

Fig. 14 presents overall heat transfer performance with channel exit height at different Darcy numbers. The result shows that the overall heat transfer performance enhances significantly at H_e = 1 and 0.5 for further increase in Darcy number at low and high Reynolds and Richardson numbers. The Darcy number has a small effect on overall heat transfer performance for convergent channel (H_e = 0.25), as shown in

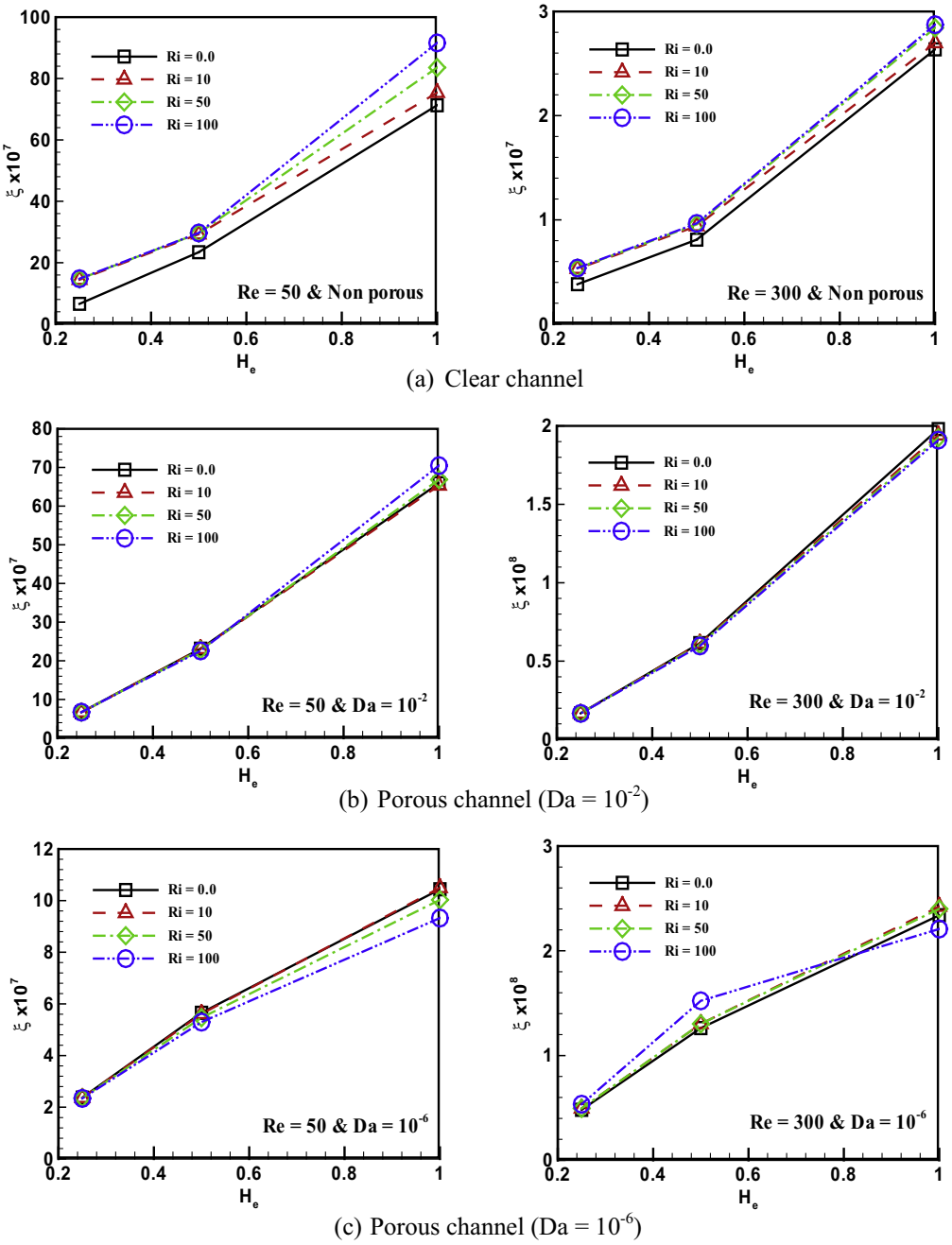

Figure 13 Variation of overall heat transfer performance with channel exit height at different Richardson numbers; (a) clear channel, (b) porous channel ($Da = 10^{-2}$), and (c) porous channel ($Da = 10^{-6}$).

Fig. 14. The straight clear channel provides the highest overall heat transfer performance at low and high Reynolds and Richardson numbers compared to straight porous channel at different Darcy numbers, whereas, the convergent clear channel with $H_e = 0.5$ and 0.25 has the same overall heat transfer performance as that provided by convergent porous channel with $Da = 10^{-2}$ at $Re = 50$ and $Ri = 0$. Moreover, the overall heat transfer performance decreases for further increase in Reynolds number and it has the highest value at low Reynolds number and high Richardson number.

4.5. Effect of Prandtl number on overall heat transfer performance and Nusselt number

Nusselt number and overall heat transfer performance of convergent porous channel ($H_e = 0.25$) at $Da = 10^{-4}$ are tested at different Prandtl numbers of 0.7, 1, 5 and 10, as shown in Fig. 15. Fig. 15a presents the effect of Richardson number on Nu and ξ along different Prandtl number at $Re = 150$. The results show that Richardson number has a small significant effect on the overall Nusselt number and overall heat

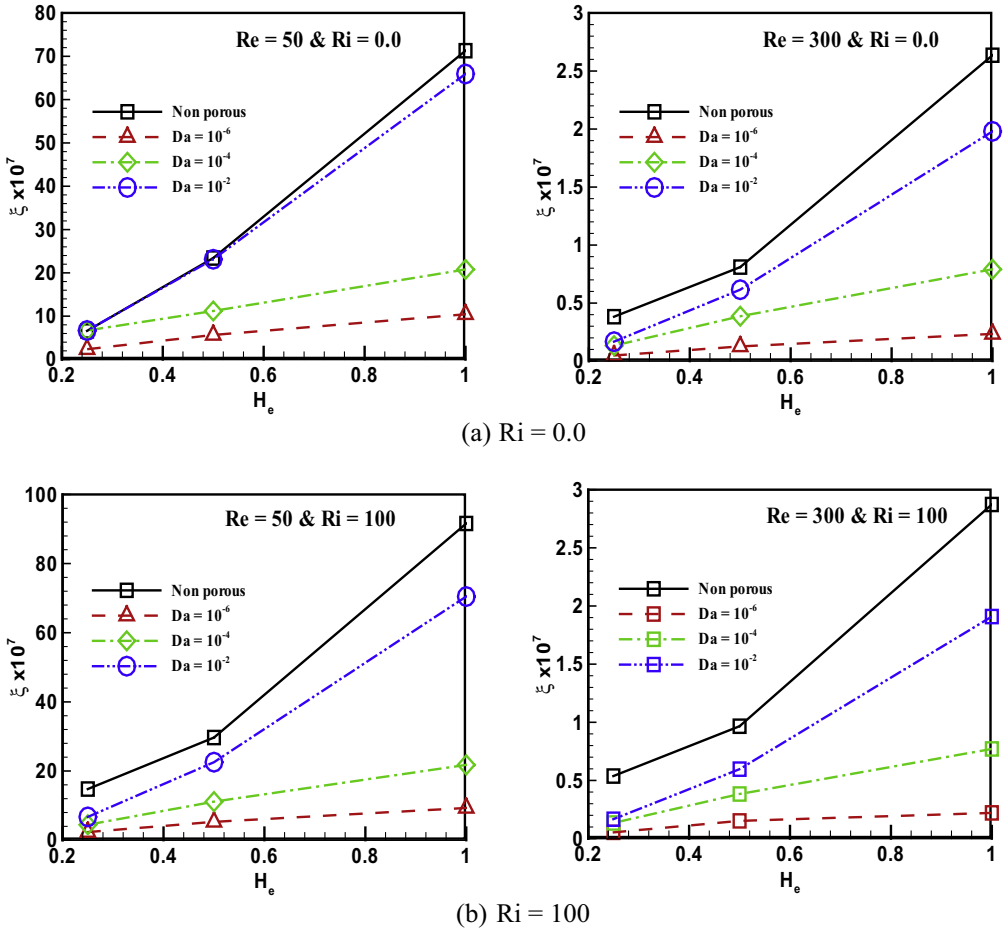

Figure 14 Variation of overall heat transfer performance with channel exit height at Darcy number; (a) $Ri = 0.0$, (b) $Ri = 100$.

transfer performances at low Prandtl number ($Pr \leqslant 1$), whereas, there is no significant effect of Richardson number for $Pr > 1$ on the overall Nusselt number and the heat transfer performance. The overall Nusselt number enhances approximately three times due to increase in Prandtl number from 0.7 to 10. The effect of Reynolds number on overall Nusselt number and ξ along different Prandtl number is illustrated in Fig. 15b. The results show that overall Nusselt number enhances by ≈50–75% and overall heat transfer performances (ξ) decrease by ≈83–87% due to increase in Reynolds number from 50 to 150 along different Prandtl numbers.

5. Conclusion

Flow-field and thermal analysis for mixing convocation of three different exit heights for clear and porous channels is investigated numerically across wide range of Reynolds, Richardson, Prandtl and Darcy numbers. Four discrete heat sources with uniform heat flux are applied at the bottom surface of the channel and the porous blocks are mounted over the heat sources with height equal to 0.5 of the local channel height. The following are the summary and conclusions drawn of the present study.

- The fluid velocity and the boundary layer thickness decrease for further increase in Richardson number for porous and clear channel, especially at low Reynolds number.
- The flow vortex at the rear porous blocks increases for decreasing the Darcy number at low and high Reynolds numbers and increases more at high Richardson number.
- The bottom surface temperature decreases for further increase in Richardson and Reynolds numbers and reducing the outlet exit height.
- The overall Nusselt number enhances for further increase in Darcy number and increases significantly for $Ri > 10$ for porous and clear channels.
- Channel height of 0.25 provides the highest Nusselt number performance and also provides the lowest overall heat transfer performance due to increase in the pressure drop across the channel.
- Richardson number has significant effect on the enhancement of the overall heat transfer performance for straight channel at low Reynolds number and high Darcy number. At $Da = 10^{-6}$, the overall heat transfer performance has the lowest values among other cases studied.
- At low Prandtl number, the Richardson number has a small significant effect on the overall Nusselt number and the heat transfer performance.

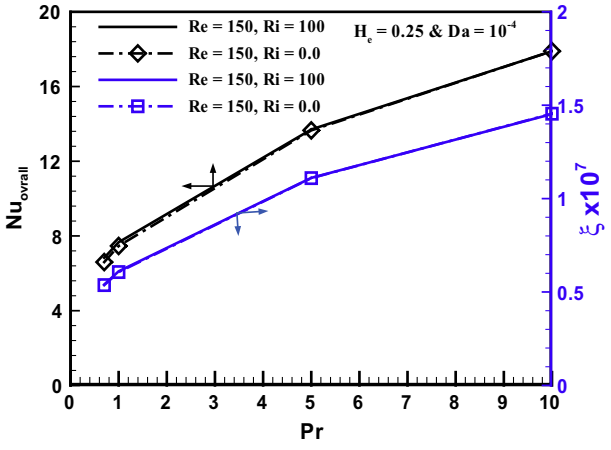

(a) Effect of Richardson number

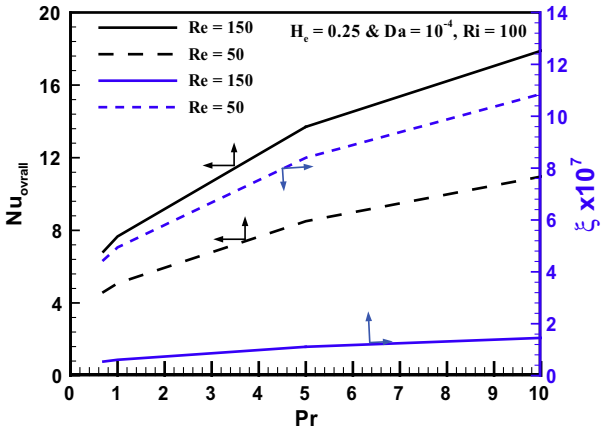

(b) Effect of Reynolds number

Figure 15 Variation of overall Nusselt number and heat transfer performance with Prandtl number; (a) Effect of Richardson number, (b) Effect of Reynolds number.

- The overall Nusselt number increases by 50–75% and overall heat transfer performance decreases from 83% to 87% due to increases in Reynolds three times (from 50 to 150).

References

[1] P. Huang, K. Vafai, Flow and heat transfer control over an external surface using a porous block array arrangement, Int. J. Heat Mass Transf. 36 (1993) 4019–4032.
[2] A. Hadim, Forced convection in a porous channel with localized heat sources, Int. J. Heat Transf. 16 (1994) 465–471.
[3] H.J. Sung, S.Y. Kim, J.M. Hyun, Forced convection from an isolated heat source in a channel with porous medium, Int. J. Heat Fluid Flow 16 (1995) 527–535.
[4] M.K. Alkam, M.A. Al-Nimr, M.O. Hamdan, Enhancing heat transfer in parallel-plate channels by using porous inserts, Int. J. Heat Mass Transf. 44 (2001) 931–938.
[5] W.S. Fu, H.C. Huang, W.Y. Liou, Thermal enhancement in laminar channel flow with a porous block, Int. J. Heat Mass Transf. 39 (1996) 2165–2175.
[6] P.X. Jiang, M.H. Fan, G.-S. Si, Z.-P. Ren, Thermal-hydraulic performance of small scale micro-channel and porous-medium heat-exchangers, Int. J. Heat Mass Transf. 44 (2001) 1039–1051.
[7] P.I. Bogdan, M.A. Abdulmajeed, An experimental and numerical study on heat transfer enhancement for gas heat exchangers fitted with porous medium, Int. J. Heat Mass Transf. 47 (2004) 4939–4952.
[8] G. Hetsroni, M. Gurevich, R. Rozenblit, Sintered porous medium heat sink for cooling of high-power mini-devices, Int. J. Heat Fluid Flow 27 (2006) 259–266.
[9] S.C. Tzeng, T.M. Jeng, Convective heat transfer in porous channels with 90-deg turned flow, Int. J. Heat Mass Transf. 49 (2006) 1452–1461.
[10] H. Shokouhmand, F. Jam, M.R. Salimpour, Simulation of laminar flow and convective heat transfer in conduits filled with porous medium using Lattice Boltzmann Method, Int. Commun. Heat Mass Transf. 36 (2009) 378–384.
[11] E.J. Javaran, S.A. Nassab, S. Jafari, Thermal analysis of a 2-D heat recovery system using porous medium including lattice Boltzmann simulation of fluid flow, Int. J. Therm. Sci. 49 (2010) 1031–1041.
[12] H.Y. Li, K.C. Leong, L.W. Jin, J.C. Chai, Analysis of fluid flow and heat transfer in a channel with staggered porous blocks, Int. J. Therm. Sci. 49 (2010) 950–962.
[13] H.W. Wu, R.H. Wang, Convective heats transfer over a heated square porous cylinder in a channel, Int. J. Heat Mass Transf. 53 (2010) 1927–1937.
[14] G. Venugopal, C. Balaji, S.P. Venkateshan, Experimental study of mixed convection heat transfer in a vertical duct filled with metallic porous structures, Int. J. Therm. Sci. 49 (2010) 340–348.
[15] T. Basak, S. Roy, A. Matta, I. Pop, Analysis of heatlines for natural convection within porous trapezoidal enclosures: effect of uniform and non-uniform heating of bottom wall, Int. J. Heat Mass Transf. 53 (2010) 5947–5961.
[16] N. Guerroudj, H. Kahalerras, Mixed convection in a channel provided with heated porous blocks of various shapes, Energy Convers. Manage. 51 (2010) 505–517.
[17] M. Ghorab, Forced Convection analysis of Discrete Heated porous convergent channel, Heat Transfer Eng. 36 (9) (2015) 829–846.
[18] A. Narasimhan, B.V. Reddy, Laminar forced convection in a heat generating bi-disperse porous medium channel, Int. J. Heat Mass Transf. 54 (2011) 636–644.
[19] S.V. Patankar, Numerical Heat Transfer and Fluid Flow, McGraw-Hill, New York, 1980.